

## RANS Based CFD Investigation of a Fuel Assembly with Local Blockage

J. H. Jeong<sup>a\*</sup>, J. Yoo<sup>a</sup>, K. L. Lee<sup>a</sup>, K. S. Ha<sup>a</sup>

<sup>a</sup> Korea Atomic Energy Research Institute, 989-111, Daedeok-daero, Yuseong-gu, Daejeon, 305-353

\*Corresponding author: jhjeong@kaeri.re.kr

### 1. Introduction

As the depletion of fossil fuels and the growing problem of spent nuclear fuel, a renewable energy has been regarded as a potential alternative energy resource. One of the major criticisms of the renewable energy is expensive and unpredictable electricity production. Sodium-cooled Fast Reactor (SFR) system would be a rapid and decisive solution for the energy crisis in the future. SFR system is one of the nuclear reactors in which a recycling of transuranics (TRUs) by reusing spent nuclear fuel sustains the fission chain reaction. This situation strongly motivated Korea Atomic Energy Research Institute (KAERI) to initiate a Prototype Gen-IV Sodium-cooled Fast Reactor (PGSFR) design project under the national nuclear R&D program.

The internal blockage in the subassembly of the SFR system is of particular importance because of tight package of the fuel bundles and the high power density. For the assessment of reactor safety in the SFR, it is necessary to understand the coolant thermal-hydraulic behaviors of the local blockage such as the vortical structures of separated flow field and the extent of overheating.

In this study, three-dimensional structures of the vortical flow field and heat transfer characteristics in the partially blocked 7-pin fuel assembly mock-up of SFR have been investigated through a numerical analysis using the commercial CFD code, CFX. Complicated and separated flow phenomena in the 7-pin fuel assembly with the central 6-subchannel blockage were captured by the RANS flow simulation with the SST turbulence model, and by the vortex structure identification technique based on the critical point theory.

### 2. Experimental Analysis Methods

An experimental study of the 7-pin fuel assembly was carried out in the sodium boiling and fuel failure propagation test loops (SIENA) installed at PNC's Oarai engineering center. Design specifications of the 7-pin fuel assembly are summarized in Table 1.

Fig. 1 and 2 show the schematic of the test section and the enlarged schematic of the blocked region by blockage plate and spacer grid. As shown in Fig. 1 and 2, an electrically heated 7-pin bundle was centered in a hexagonal tube, with a 24 mm flat-to-flat distance inside. The heated pins were 6.5 mm in diameter, arranged in a triangular array with pin pitch of 7.9 mm, and had a 450 mm heated length. The pitch-to-diameter ratio (P/D)

was 1.22. The central 6-subchannel blockage plate was welded at a distance of 350 mm from the start of the heated section on the upstream side of the grid spacer. The blockage plate area ( $0.63 \times 10^{-4} \text{ m}^2$ ) and grid spacers area ( $0.61 \times 10^{-4} \text{ m}^2$ ) blocked 23.6 %, 22.8 % of the total flow area ( $2.67 \times 10^{-4} \text{ m}^2$ ), respectively.

Table 1. Test section geometry parameters

Geometry parameters	Test section
Number of pins	7
Pin diameter (mm)	6.5
Pin pitch (mm)	7.9
Heated length (mm)	450
Heat flux distribution	Uniform
Blockage type	Central
Thickness of blockage plate (mm)	0.5
Outer diameter of grid spacer (mm)	7.9
Height of grid spacer (mm)	5.0
Blockage location (mm)	350
Tube flat-to-flat distance (mm)	24
Blockage area fraction (%)	42
Spacing of the grid spacers (mm)	200

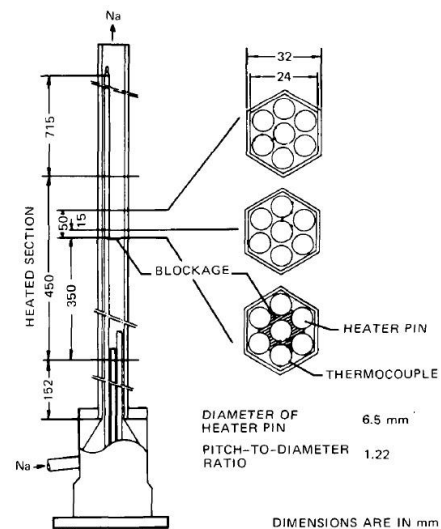


Fig. 1. Schematic of the test section (Daigo et al.<sup>(1)</sup>)

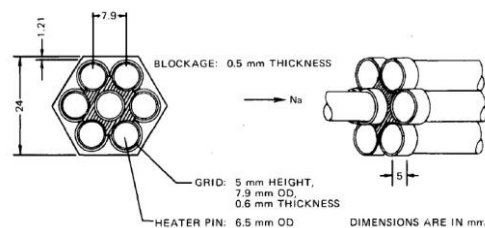


Fig. 2. Enlarged schematic of the centrally blocked region by blockage plate and grid spacer (Daigo et al.<sup>(1)</sup>)

### 3. Numerical Analysis Methods

The present investigation of CFD was carried out over the full scale experimental facility of SIENA's 7-pin fuel assembly. Fig. 3 shows the test section of numerical analysis. Fig. 4 shows the enlarged schematic around the blockage plate and grid spacers in the 7-pin fuel assembly. The blockage of the test section is composed with the heated section of 450 mm, blockage plate with the thickness of 0.5 mm, and grid spacers with the thickness of 5.0 mm. Numerical meshes are highly concentrated around the blockage region to capture the details of the recirculation such as wake behind the blockage plate and grid spacers. As shown in Fig. 4, the axial length scale of computational mesh is axially 0.05 mm and 0.5 mm in the blockage plate and grid spacers, respectively.

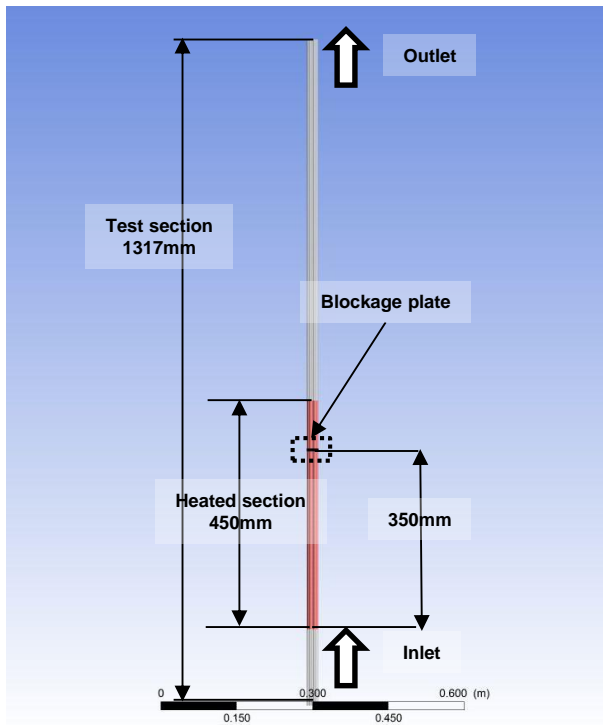


Fig. 3. Test section of numerical analysis

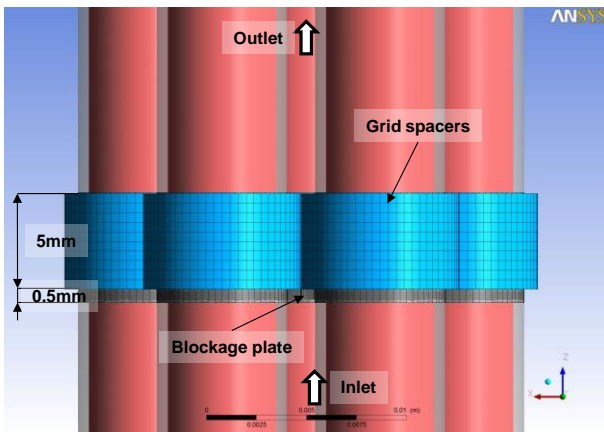


Fig. 4. Enlarged schematic near the blockage plate and grid spacers

The computational grid system is composed of structured meshes. Table 2 describes the computational grids system. As shown in table 2, the computational grids system divided into two regions of the fluid part and structure part. The total number of the computational grids system was approx.  $2.78 \times 10^6$  cells.

Table 2. Computational grids system

7-Pin	Cells	Nodes	Elements
Fluids	1,583,790	1,646,330	1,583,790
Structures	1,192,100	1,341,340	1,192,100
Total	2,775,890	2,987,670	2,775,890

Table 3 describes the computational boundary condition of the CFD analysis. As shown in table 3, inlet and outlet are defined with constant velocity of 4.92 m/s and temperature of 556.25 K, and relative pressure of 0 Pa, respectively. Inner cladding domain of the heated section has constant heat flux of 660 kW/m<sup>2</sup>. Outer cladding, wire, blockage plate, and grid spacers are defined with no slip condition, conservative interface flux, and smooth roughness. Duct wall is applied to no slip and adiabatic condition.

Table 3. Boundary condition in the 7-pin fuel assembly

Boundary domain	Condition	Value
-Inlet	-Constant velocity	4.92 [m/s]
	-Constant temperature	556.25 [K]
-Outlet	-Relative pressure	0 [Pa]
-Inner cladding (Heat source)	Constant heat flux	660 [kW/m <sup>2</sup> ]
-Outer cladding (=rod) and wire	-No slip	-
-Blockage plate	-Conservative interface flux	-
-Grid spacers	-Smooth wall	-
-Duct Wall	-No slip	-
	-Adiabatic	-

### 4. Numerical Analysis Results

#### 4.1 Comparison of CFD with EXP

Comparison of the CFD analysis results with the experimental results in the 7-pin fuel assembly was carried out to validate the CFD analysis results. Table 4 shows an inlet and outlet temperature of the experimental and CFD analysis results. As you shown in table 4, the inlet temperature difference between the experimental and CFD analysis results is same, and the outlet temperature difference between experimental and CFD analysis results is different about 1.85 K. This temperature difference would be induced by the reduction method of temperature data. The temperature of the experiment is obtained by measuring some of

temperatures of the outlet region. However, the temperature of the CFD analysis is calculated by the area-averaged method.

Fig. 5 shows the axial wall temperature distribution behind the 6-subchannel central blockage. The vertical axis in Fig. 5 is the wall temperature measured by the thermocouples with 0.3mm diameter at the center pin  $0^\circ$ , the outer pin  $0^\circ$ , the outer  $60^\circ$ , and the outer  $120^\circ$  angular position. The horizontal axis in Fig. 5 is the axial distance from the blockage location. As shown in Fig. 5, the CFD analysis results have a good agreement with the experiment results except for the blockage region. The temperatures of the CFD analysis at the center pin  $0^\circ$ , the outer pin  $60^\circ$ , and the outer pin  $120^\circ$  angular position increase with the increasing distance from the blockage plate to the grid spacers. Above phenomenon would be related to the fact that the grid spacers also induce the partially strong blockage effect on the flow fields.

Table 4. Inlet and outlet temperature of experiment and CFD analysis results

	Experimental results	CFD results
Inlet temperature [K]	556.25	556.25
Outlet temperature [K]	576.40	578.25

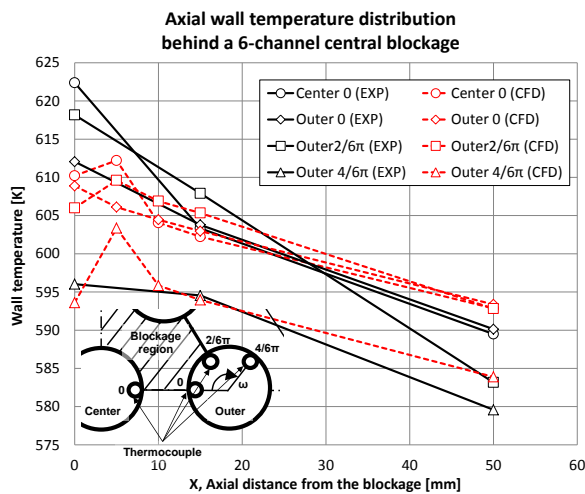
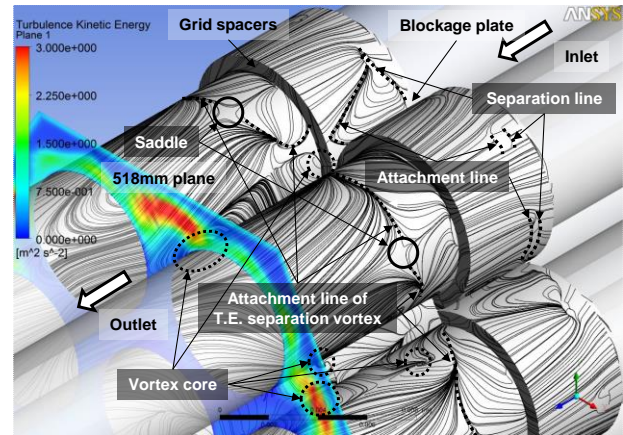


Fig. 5. Temperature comparison of the experimental results and the CFD analysis results

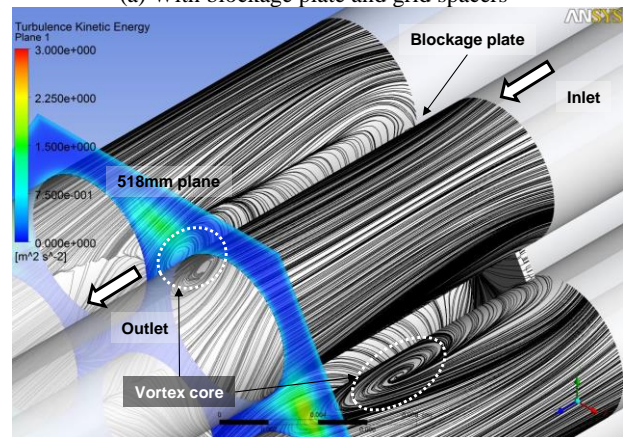
#### 4.2 Three-dimensional Flow Field

To investigate the vortex structures in the complex wake flow fields, the limiting streamline analysis based on the critical-point theory<sup>(6)</sup> was carried out. Fig. 6 shows the limiting streamline on the wall surface and the turbulence kinetic energy distribution on the cross sectional planes of the axial direction. Fig. 6 (a) is the CFD analysis results with the blockage plate and grid spacers. Fig. 6 (b) is the CFD analysis results with the blockage plate and without the grid spacers. Fig. 6 (c) is the CFD analysis results without the blockage plate and

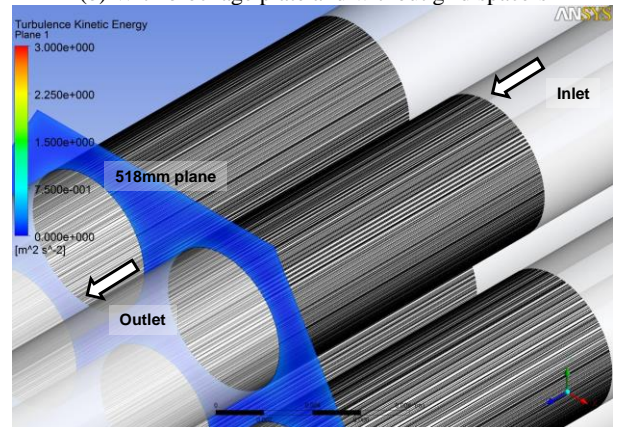
grid spacers. Vortical flow field in Fig. 6 (a) is far more complicated than that in Fig. 6 (b) and (c). As shown in Fig. 6 (a), a boundary layer is axially developing along the rod bundle, and then the boundary layer is separated behind the blockage plate and the grid spacers. Locally separated vortex on the wall surface of the grid spacer in the outer sub-channel starts to be formed from 10 % to 20 % span-wise position of the grid spacers. The separated vortex on the wall surface of the grid spacer attaches from 30 % to 90 % span-wise position of the grid spacers. Truncated section of the end of the grid spacer generates a wake vortex. The wake vortex is



(a) With blockage plate and grid spacers



(b) With blockage plate and without grid spacers



(c) Without blockage plate and grids spacers

Fig. 6. Limiting streamline on the wall surface and turbulence kinetic energy distribution on the cross sectional planes

attached at the downstream of 50 % of the grid spacer length. Regardless of the locally separated vortex generated on the grid spacer surface, a large-scale vortex generated by the blockage plate in Fig. 6 (a) and (b) is still developing, which is having the vortex core around the plane of 518 mm. Compared to Fig. 6 (a) with Fig. 6 (b), the small-scale and large-scale vortex generated by the grid spacers and blockage plate in Fig. 6 (a) has higher turbulence kinetic energy than that in Fig. 6 (b), respectively. Generally, the pressure loss is largely caused by dissipation of turbulence kinetic energy into heat. Based on the analysis of three-dimensional flow field, it is expected that the pressure loss caused by the large-scale vortex behavior of Fig. 6 (a) is larger than that of Fig. 6 (b).

#### 4.3 Heat Transfer Characteristics

To understand the details of heat transfer characteristics in the thermal wake region, Nusselt number was evaluated by the CFD analysis results. Fig. 7 shows the axial Nusselt number distribution around the 6-subchannel central blockage. The vertical axis in Fig. 7 is the Nusselt number calculated by the length-averaged wall surface temperature and the area-averaged bulk temperature on the cross sectional plane at the axial position from blockage. As shown in Fig. 7, the Nusselt number dramatically decreases at the 5 mm blockage downstream. As going to blockage downstream, the Nusselt number goes on increasing again. Compared with the Nusselt number with only blockage plate, the Nusselt number with the blockage plate and grid spacers is remarkably increasing behind blockage region. That is the reason why the grid spacers just behind the blockage plate generate the small-scale vortex structures with high turbulence kinetic energy. As these vortex structures go on downstream and are mixed with the flow of the outer sub-channels in Fig. 7 (a), the heat transfer characteristics are enhanced.

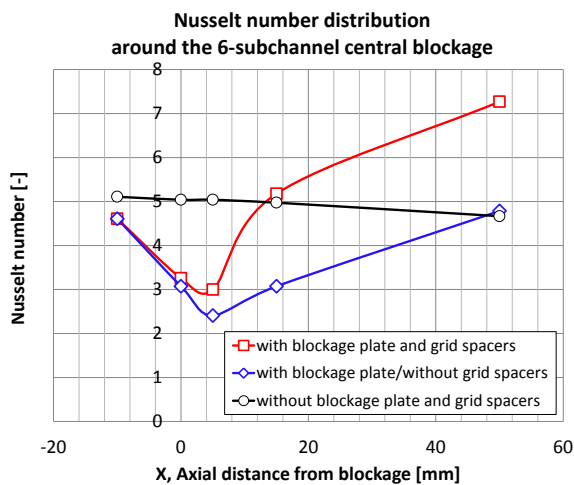
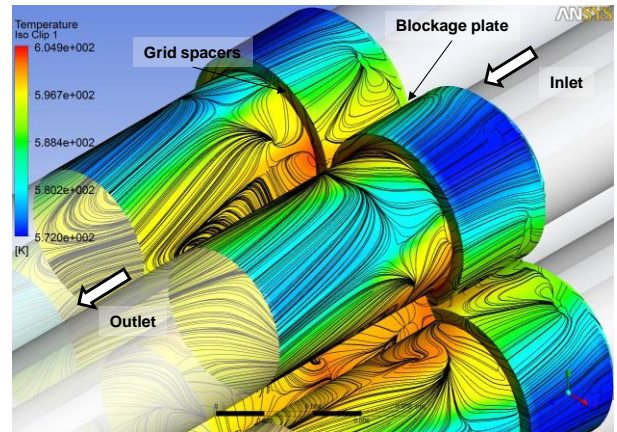
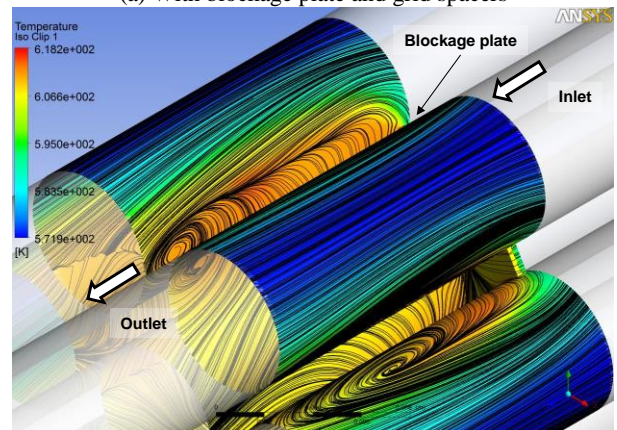


Fig. 7. Axial Nusselt number distribution around the central blockage

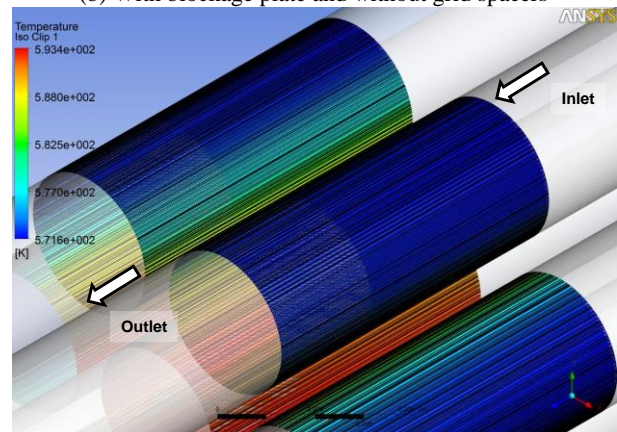
Fig. 8 shows the temperature distribution and limiting streamline on the wall surface. As shown in Fig. 8 (a), (b), and (c), the temperature distribution on the wall surface is closely related to the limiting streamline on the wall surface. Based on the critical point theory, the limiting streamline with the vortex core has the highest cladding wall temperature, and the limiting streamline with the attachment line has a low cladding wall temperature. As previously mentioned, the limiting streamline is formed by the vortex structure behavior. The large-scale vortex structures supply the thermal energy from downstream near the heated outer cladding



(a) With blockage plate and grid spacers



(b) With blockage plate and without grid spacers



(c) Without blockage plate and grids spacers

Fig. 8. Temperature distribution and limiting streamline on the rod wall surface

wall surface to upstream of the blockage plate. For this region, the cladding wall surface temperature near the blockage plate and grid spacer is higher than that of other axial positions. The vortex structure behavior significantly dominates the heat transfer characteristics.

#### **4. Conclusions**

Three-dimensional structures of a vortical flow field and heat transfer characteristics in the partially blocked 7-pin fuel assembly mock-up of SFR have been investigated through a numerical analysis using a commercial CFD code, CFX. Complicated and separated flow phenomena in the 7-pin fuel assembly with a central 6-subchannel blockage were captured by RANS flow simulation with the SST turbulence model, and by a vortex structure identification technique based on the critical point theory. The conclusions are as below.

1. Three-dimensional multi-scale vortex structures start to be formed around the central blockage plate and grid spacer, and develop in the axial direction.
2. Large-scale vortex structures and small-scale vortex structures, which are respectively generated by the blockage plate and grid spacer, dominate the heat transfer characteristics. Compared to the CFD results without a grid spacer, small-scale vortex structures by the grid spacer significantly enhance the convective heat transfer because the small-scale vortex structures tend to accelerate turbulent mixing and make the turbulence kinetic energy increase.

#### **ACKNOWLEDGEMENTS**

This work has been performed under the nuclear R&D program supported by the Ministry of Science, ICT and Future Planning of the Republic of Korea.

#### **REFERENCES**

- [1] Y. Daigo, et al., Local Temperature Rise due to a 6-Channel Blockage in a 7-Pin Bundle, *JAPFNR-202*, 1975.
- [2] K. Haga, et al., The Effects of Bowing Distortions on Heat Transfer in a Seven-pin Bundle, *ASME 1974 Winter Annual Meeting*, New York, NY, USA, November 18-22, 1974.
- [3] J. Smagorinsky, General Circulation Experiments with the Primitive Equations. I. The Basic Experiment, *Mon. Weather Rev.*, 91, pp. 99-165, 1963.
- [4] D. C. Wilcox, Reassessment of the Scale-determining Equation for Advanced Turbulence Models, *AIAA Journal*, 26(11), pp.1299-1310, 1998.
- [5] F. R. Menter, Two-equation eddy-viscosity turbulence models for engineering applications, *AIAA Journal*, 32(8), pp. 1598-1605, 1994.
- [6] A. E. Perry and M. S. Chong, A Description of Eddy Motions and Flow Patterns Using Critical-Point Concepts, *Annual Review of Fluid Mechanics*, 19, pp. 125-155, 1987.